stable hydrogen bonds are Ile66, Ala71, Gln92, and Ile93 with His69 in the WT; Pro1, Ile66, Cys67, Gly68, and Lys70 with Asn69 in the mutant.

We also analyzed the impact of the mutations on the active-site residue Asp25 by examining the stable hydrogen bonds formed by this residue in the four simulated systems. In the WT we observed eleven stable hydrogen bonds between the main and side chain of Asp25 in both monomers, involving residues Arg8, Leu23, Thr26, Gly27, Ala28, and Ile85. In T12A, fourteen hydrogen bonds exceed the 60% simulation-time threshold, between Asp25 and Arg8, Thr26, Gly27, Ala28, and Ile85. In L63Q, ten stable hydrogen bonds are formed between Asp25 and Arg8, Thr26, Gly27, and Ala28. H69N shows thirteen stable hydrogen bonds between Asp25 and Arg8, Leu23, Thr26, Ala28, and Ile85.

All mutations, therefore, preserve key stable interactions between Asp25 and the three residues Arg8, Thr26, and Ala28. Three additional residues form stable interactions with Asp25, but not in all systems: Leu23 in WT and H69N; Gly27 in all systems except H69N; and Ile85 in all systems except L63Q. The nature of these interactions further contributes to the dynamic structure of the active site, with some hydrogen bonds not reaching the 60% threshold because they switch donor or acceptor atoms. For example, the interactions between Arg8 NH2 and Asp25 OD1 and Asp25 OD2 are present for 39% and 27% of the simulation time, respectively.

2.6. Long Range Correlated Motions

We further investigated long-range interactions in HIV-1 PR by building Dynamic Cross-Correlation Maps (DCCMs) from the concatenated three trajectories (last 450 ns of each replica). Highly positive values of the map elements (Cij) indicate a strong correlation between the motions of residues i and j (colored in green, yellow, and red in Figure 6), whereas negative Cij values denote that the two residues move in opposite directions (anti-correlated motion; colored in cyan, light blue, and dark blue in Figure 6). Both correlated and anti-correlated motions are relevant when investigating biological macromolecules, particularly when residues are located far apart in the protein sequence.

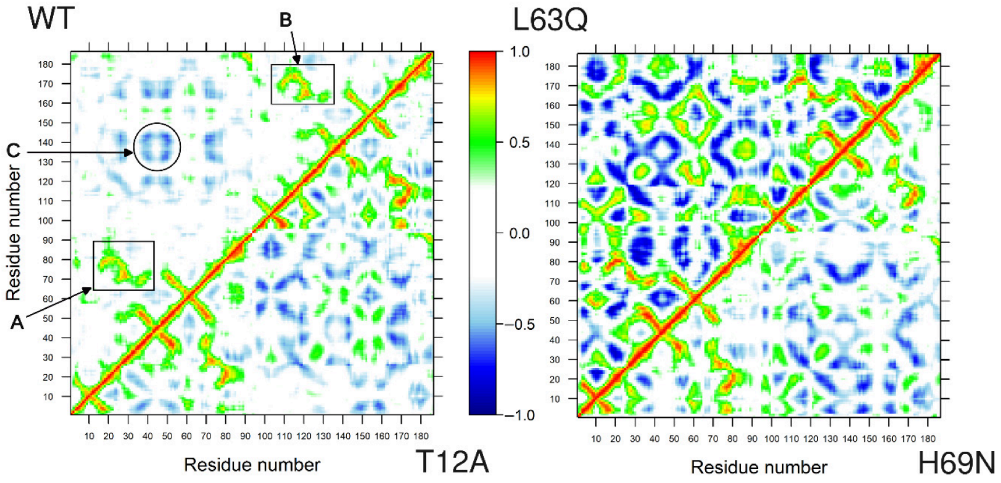

Figure 6. Comparison of dynamic cross-correlation maps for native (upper left triangle) and T12A system (lower right triangle), and L63Q (upper left triangle) and H69N system (lower right triangle). Specific regions are highlighted with rectangles A, B and circle C.

This analysis shows that, in the native protease, long-range correlated motions are established that are functionally linked to the biological role of PR. In particular, strong correlations are observed between residues 12–43 (encompassing the Fulcrum, Fireman's Grip, and Elbows) and residues 65–90 (corresponding to the Cantilever β-sheet, the Wall, and the α-helix) in monomer 1, and the equivalent regions in monomer 2, highlighted by

rectangles A and B, respectively, in Figure 6. These correlated motions connect the active-site region with the central, structured core of PR. In the native system, anti-correlated motions between the two flap regions are also evident, highlighted by circle C in Figure 6.

To facilitate comparison of the correlated motions highlighted by rectangles A and B in Figure 6 for the WT with the corresponding regions in the mutants, we extracted these regions from the DCCM, together with the correlated motions between the two flaps (circle C in Figure 6), and present them in Figure 7. The pattern of correlated motions in regions A and B is clearly preserved across all systems. Notably, the flap regions, shown in C, consistently exhibit anti-correlated motions, which are more pronounced in L63Q than in the WT, and less pronounced in T12A and H69N.

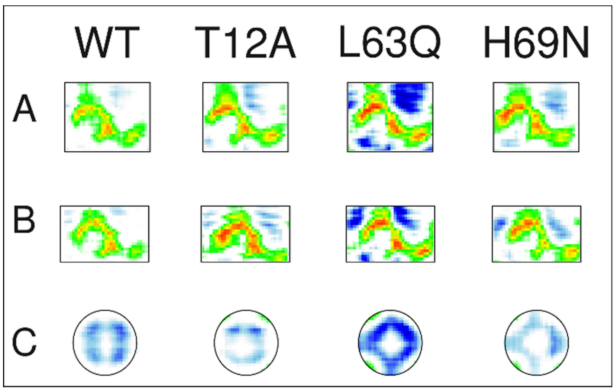

Figure 7. Comparison of the region enclosed in rectangles A, B and circle C in WT of the DCCM of Figure 6 with the corresponding regions in the mutants. Colors as in Figure 6.

Overall, the T12A mutation in the Fulcrum and the L63Q and H69N mutations in the Cantilever do not disrupt the native long-range network of correlated motions, but they do introduce a large number of additional correlated and anti-correlated motions in other regions of PR (see Figure 6). This increase is particularly pronounced in the L63Q mutant.

3. Discussion

In this molecular dynamics study, we investigated the effects of three mutations (T12A, L63Q, and H69N) on the structure and dynamics of HIV-1 protease. Overall, the results indicate that none of the mutations induces a global structural destabilization of the enzyme, consistent with their natural occurrence.

Notably, the lack of major changes in the overall enzyme structure agrees with previous structural and biochemical studies showing that HIV-1 protease preserves its global fold even in highly drug-resistant variants [6,9]. This highlights the remarkable structural robustness of the enzyme and suggests that resistance is often driven by subtle dynamic changes rather than large-scale structural rearrangements.

All systems preserve their secondary structure throughout the 500 ns simulations and across all replicas (see Figures 5 and S4–S15), as well as key contacts in the active site and the main long-range interdomain correlated motions observed in the wild-type system (see Figure 7). However, despite this apparent structural stability, the mutations markedly modulate the internal dynamics of the protease, particularly affecting flap mobility, hydrogen bond networks, and long-range correlated motions involving the entire protein.

RMSD analyses show that all mutant systems sample conformational states that deviate more from the starting structure than the native protease. This effect is particularly pronounced for T12A, which exhibits consistently higher RMSD values across all replicas (see Figure 2 and Table 1). Importantly, this increase is not solely attributable to flap motion. Even after excluding flap residues from the calculation, mutants still

display larger deviations than the native system, indicating that the mutations reshape the global conformational landscape of HIV-1 PR rather than inducing only localized perturbations (see Figure 3 and Table 2).

RMSF analyses further reveal mutation-specific effects on protein flexibility (see Figure 4). As expected, the largest fluctuations occur within the flap domains (residues 43–58) in all systems and both monomers, confirming their intrinsic flexibility and functional relevance. In the native protease, the flap dynamics exhibit pronounced asymmetry between the two monomers, a feature previously associated with functional opening and closing mechanisms [25]. This asymmetry is preserved but reshaped in the mutant systems. A common feature is the anti-correlated motion between the two flaps even though with different magnitude (see C in Figure 7).

In particular, T12A shows increased flexibility in regions outside the flaps, including residues adjacent to the catalytic site (e.g., Gly27), suggesting an enhanced coupling between local active-site dynamics and distal structural regions. In contrast, L63Q exhibits an overall stabilizing effect, with reduced fluctuations both within and outside the flap domains, while H69N displays an intermediate behavior with localized modulation of flexibility.

The functional relevance of these dynamical differences is further supported by the analysis of flap opening, monitored through the inter-monomer distance between the c-alpha atoms of Ile50. All systems sample open-flap conformations, confirming that flap opening is an intrinsic dynamic feature of HIV-1 PR. However, both the frequency and extent of these conformations are mutation-dependent. T12A and H69N exhibit a clear shift toward more open states compared to the native enzyme, whereas L63Q samples open conformations less frequently.

These findings indicate that mutations in the fulcrum (T12A) and cantilever (H69N) regions can enhance flap opening, potentially increasing active-site accessibility, whereas L63Q appears to restrict flap motion. The lack of a simple correlation between flap opening and global RMSD further suggests that the flap dynamics are governed by a complex interplay of local and long-range interactions rather than by isolated structural elements.

Analysis of stable hydrogen bonds shows that each mutation induces a distinct local reorganization of interaction networks without disrupting the catalytic core. T12A markedly reduces the number of stable hydrogen bonds at the mutation site, increasing local flexibility in the fulcrum region. Conversely, L63Q introduces an extensive hydrogen bond network, consistent with its stabilizing effect on both local and global dynamics. H69N produces a hydrogen bonding pattern more similar to the native system, explaining its intermediate behavior.

Despite these local rearrangements, key interactions involving the catalytic residue Asp25 are preserved across all systems. Stable hydrogen bonds between Asp25 and residues such as Arg8, Thr26, and Ala28 are maintained, indicating that the fundamental architecture of the active site remains intact. Thus, the mutations modulate the dynamic environment of the catalytic site without compromising its structural integrity, supporting a mechanism of functional regulation through dynamical tuning rather than structural disruption.

Dynamic cross-correlation analyses provide further insight into the impact of the mutations on global communication pathways within HIV-1 PR. In the native protease, well-defined networks of correlated motions connect the Fulcrum, Hinge, Flap, and Cantilever regions across both monomers, linking the active site to distal structural elements. These long-range correlations are thought to be essential for coordinated flap motion and enzymatic function [20,22,26].

All three mutations preserve the overall framework of correlated motions but introduce additional correlated and anti-correlated movements throughout the protein. This effect

is particularly pronounced in L63Q, which displays an expanded network of long-range correlations, consistent with its enhanced structural rigidity and reduced flap mobility.

Taken together, these results indicate that mutations in the fulcrum and cantilever regions of HIV-1 PR act as dynamic modulators rather than structural disruptors. T12A promotes increased conformational variability and enhanced flap opening, potentially facilitating substrate access while altering active-site coupling. L63Q stabilizes the protease by reinforcing hydrogen bond networks and long-range correlations, resulting in reduced flap mobility. H69N exhibits mixed behavior, maintaining native-like hydrogen bonding while shifting the flap dynamics toward more open conformations.

Overall, this mutation-dependent tuning of protein dynamics highlights the critical role of distal regions in regulating HIV-1 PR function and provides a mechanistic framework for understanding how non-active-site mutations can exert long-range effects on protein region involved in enzymatic activity, potentially contributing to drug sensitivity through dynamic modulation rather than direct structural alterations.

4. Materials and Methods

4.1. Structure Preparation and Mutant Generation

The experimentally determined structure of the Native HIV-1 PR [PDB ID: 1ODW] was retrieved from the RCSB Protein Data Bank (https://www.rcsb.org/) for our study [27]. The ligand di-tert-butyl {iminobis[(2S,3S)-3-hydroxy-1-phenylbutane-4,2-diyl]}biscarbamate (chain C) was removed from the native structure to create a model to use in the MD simulations. Chimera's Rotamers tool, using Dunbrack backbone-dependent rotamer library, was used to replace the native residues in the HIV-1 protease structure in an equilibrated native MD structure (see following paragraph) and create mutant structures for MD simulations [28]. The residue rotamer with the highest probability (if required) was chosen for each mutant protease model.

4.2. Molecular Dynamics Simulations

Topology files for MD simulations were created with the GROMACS gmx pdb2gmx tool [29]. Protonation states of ionizable residues were assigned assuming physiological pH (~7.0). The HIV-1 PR system was added into a cubic box with a minimum distance of 1.0 nm between the protein and the box edges, solvated with water (TIP3P water model) [30] and neutralized with the addition of ions using the GROMACS tools: editconf, solvate and genion, respectively. Charmm 36 force field was used to describe the system during the MD protocol [31]. The protein simulation box was minimized with both the steepest descent algorithm, followed by the conjugate gradient algorithm, until convergence was achieved. After that, 5 ns of MD simulation with GROMACS 2020.3 were produced with a 2 fs time step by applying positional restraints of 1000 kJ mol^{-1} nm^{-2} to the protein atoms. This equilibrated structure was used to create the mutant starting structure, and the same equilibration protocol was used for these systems.

Unrestrained MD simulations of the four systems were carried out with GROMACS 2020.3 for 500 ns each with a 2 fs time step, using the Linear Constraint Solver (Lincs) algorithm [32] on the High-Performance Computing Leonardo system at CINECA center, Bologna, Italy, and using the bioinformatics Elixir-IT resources on g100 at CINECA for the analysis [33].

Long-range electrostatic interactions were treated using the Particle Mesh Ewald (PME) method [34]. During the simulation, a constat temperature of 300 K was maintained using the velocity rescaling thermostat [35], and pressure was kept constant at 1 bar using the Rahman–Parrinello barostat [36].

4.3. Analyses of Trajectory Files

To assess trajectory quality and verify convergence of the protein systems toward equilibrium, the root-mean-square deviation (RMSD) was calculated with respect to the first frame of each trajectory, using the GROMACS gmx rms tool. Global stability was evaluated from c-alpha RMSD values over the 500 ns simulations, including calculations performed both with and without the flap region (residues 43–58), in order to distinguish overall conformational changes from flap-specific motions.

Residue-level flexibility was characterized by using RMSF profiles to identify mutation-induced changes in local dynamics, using the GROMACS gmx rmsf tool. Finally, flap opening was monitored by measuring the c-alpha–c-alpha distance between Ile50 residues of the two monomers, and considering the state open for distances greater of 1 nm, allowing quantification of the population of open conformations across replicas and systems. This is the most widely validated metric to define the conformational state of the HIV-1 PR flaps [20–22].

Residence times (τ) were calculated as the average time spent in each state between consecutive transitions, following standard kinetic analysis of discrete-state trajectories and Markov-state-model frameworks [23,24], and considering the percentage of time spent in the open state in each trajectory.

The secondary structure analysis was performed using a custom Python v3 script based on the MDAnalysis library [37], which interfaces with the Define Secondary Structure of Proteins (DSSP) algorithm to assign secondary structure elements to each residue along the MD trajectories [38]. For each system (WT, T12A, L63Q, and H69N), DSSP assignments were extracted frame by frame and grouped into three main categories—helix, β-sheet, and coil. The residue-wise secondary structure propensities were then calculated by averaging over the entire simulation time and across three independent replicas, providing a robust comparison of structural stability and local conformational preferences among the variants.

Hydrogen bonds were calculated using GROMACS gmx hbond tools, with standard geometrical criterion: i.e., distance between the donor and the acceptor less than 0.35 nm; hydrogen-donor-acceptor angle minor less than 30°. A hydrogen bond was considered "stable" when present for more than 60% of simulation time. DCCM (Dynamical Cross-Correlation Matrix) were calculated using the dccm() function in the Bio3D R package [39].

5. Conclusions

Several classes of antiretroviral drugs are currently available for the treatment of HIV infection, including nucleoside and non-nucleoside reverse transcriptase inhibitors, as well as viral protease inhibitors. The introduction of protease inhibitors into highly active antiretroviral therapy (HAART) has markedly reduced morbidity and mortality, significantly improving the life expectancy of people living with HIV. Understanding the structural and dynamical effects of protease mutations therefore remains essential for elucidating mechanisms that may influence enzymatic function and therapeutic response.

In this molecular dynamics study, we investigated the effects of the T12A, L63Q, and H69N mutations on the structure and dynamics of HIV-1 protease. All variants preserve the global fold, compactness, and secondary structure of the enzyme, indicating that these mutations do not induce significant structural destabilization.

Despite this overall stability, the mutations modulate the internal dynamics of the protease in a mutation-specific manner. T12A and H69N promote increased sampling of open-flap conformations, whereas L63Q reduces flap mobility. These effects are accompanied by distinct rearrangements of local hydrogen bond networks and alterations in long-range correlated motions, while key catalytic interactions involving Asp25 remain conserved.

Overall, the results indicate that mutations in the Fulcrum and Cantilever regions act as dynamic modulators rather than structural disruptors, reshaping the conformational landscape of HIV-1 protease and potentially influencing enzymatic function through changes in protein dynamics.

Supplementary Materials: The following supporting information can be downloaded at: https://www.mdpi.com/article/10.3390/ijms27093832/s1.

Author Contributions: Conceptualization, G.C., N.A. and H.S.; methodology, G.C., N.A. and H.S.; formal analysis G.C., N.A., C.P. and H.S.; investigation, H.S., G.C., L.F. and N.A.; writing, all authors; funding acquisition, G.C. All authors have read and agreed to the published version of the manuscript.

Funding: This research received no external funding.

Data Availability Statement: Dataset available on request from the authors.

Acknowledgments: We acknowledge Cineca and Elixir-IT computational resources and Tunisian Ministry of Higher Education.

Conflicts of Interest: The authors declare no conflicts of interest.

Abbreviations

AIDS	Acquired Immunodeficiency Syndrome
HAART	Highly active antiretroviral therapy
HIV	Human Immunodeficiency Virus
MD	Molecular dynamics
PDB	Protein Data Bank
PLH	people living with HIV
PR	Protease
RMSD	Root-mean-square deviation
RMSF	Root-mean-square fluctuation
RT	Reverse transcriptase
WT	Wild type

References

1. Bebenek, K.; Abbotts, J.; Roberts, J.D.; Wilson, S.H.; Kunkel, T.A. Specificity and mechanism of error-prone replication by human immunodeficiency virus-1 reverse transcriptase. *J. Biol. Chem.* **1989**, *264*, 16948–16956. [CrossRef]
2. May, M.; Gompels, M.; Delpech, V.; Porter, K.; Post, F.; Johnson, M.; Dunn, D.; Palfreeman, A.; Gilson, R.; Gazzard, B.; et al. Impact of late diagnosis and treatment on life expectancy in people with HIV-1: UK Collaborative HIV Cohort (UK CHIC) Study. *BMJ* **2011**, *343*, d6016. [CrossRef]
3. May, M.T.; Gompels, M.; Delpech, V.; Porter, K.; Orkin, C.; Kegg, S.; Hay, P.; Johnson, M.; Palfreeman, A.; Gilson, R.; et al. Impact on life expectancy of HIV-1 positive individuals of CD4+ cell count and viral load response to antiretroviral therapy. *AIDS* **2014**, *28*, 1193–1202. [CrossRef] [PubMed]
4. Palella, F.J.; Delaney, K.M.; Moorman, A.C.; Loveless, M.O.; Fuhrer, J.; Satten, G.A.; Aschman, D.J.; Holmberg, S.D. Declining morbidity and mortality among patients with advanced human immunodeficiency virus infection. *N. Engl. J. Med.* **1998**, *338*, 853–860. [CrossRef]
5. Navia, M.A.; Fitzgerald, P.M.D.; McKeever, B.M.; Leu, C.T.; Heimbach, J.C.; Herber, W.K.; Sigal, I.S.; Darke, P.L.; Springer, J.P. Three-dimensional structure of aspartyl protease from human immunodeficiency virus HIV-1. *Nature* **1989**, *337*, 615–620. [CrossRef] [PubMed]
6. Wlodawer, A.; Vondrasek, J. Inhibitors of HIV-1 protease: A major success of structure-assisted drug design. *Annu. Rev. Biophys. Biomol. Struct.* **1998**, *27*, 249–284. [CrossRef]
7. Clavel, F.; Hance, A.J. HIV drug resistance. *N. Engl. J. Med.* **2004**, *350*, 1023–1035. [CrossRef]
8. Zazzi, M.; Hu, H.; Prosperi, M. The global burden of HIV-1 drug resistance in the past 20 years. *PeerJ* **2018**, *6*, e4848. [CrossRef] [PubMed]
9. Weber, I.T.; Agniswamy, J. HIV-1 protease: Structural perspectives on drug resistance. *Viruses* **2009**, *1*, 1110–1136. [CrossRef]
10. Kuritzkes, D.R. Drug resistance in HIV-1. *Curr. Opin. Virol.* **2011**, *1*, 582–589. [CrossRef]

11. Heaslet, H.; Kutilek, V.; Morris, G.M.; Lin, Y.-C.; Elder, J.H.; Torbett, B.E.; Stout, C.D. Structural insights into the mechanisms of drug resistance in HIV-1 protease NL4-3. *J. Mol. Biol.* **2006**, *356*, 967–981. [CrossRef] [PubMed]
12. Engelman, A.; Cherepanov, P. The structural biology of HIV-1: Mechanistic and therapeutic insights. *Nat. Rev. Microbiol.* **2012**, *10*, 279–290. [CrossRef]
13. Dakshinamoorthy, A.; Asmita, A.; Senapati, S. Comprehending the structure, dynamics, and mechanism of action of drug-resistant HIV protease. *ACS Omega* **2023**, *8*, 9748–9763. [CrossRef] [PubMed]
14. Sadiq, S.K.; De Fabritiis, G. Explicit solvent dynamics and energetics of HIV-1 protease flap opening and closing. *Proteins Struct. Funct. Bioinform.* **2010**, *78*, 2873–2885. [CrossRef] [PubMed]
15. Weber, I.T.; Kneller, D.W.; Wong-Sam, A. Highly resistant HIV-1 proteases and strategies for their inhibition. *Future Med. Chem.* **2015**, *7*, 1023–1038. [CrossRef]
16. Huang, L.; Sayer, J.M.; Swinford, M.; Louis, J.M.; Chen, C. Modulation of HIV-1 protease autoprocessing by charge properties of surface residue 69. *J. Virol.* **2009**, *83*, 7789–7793. [CrossRef]
17. Suñé, C.; Brennan, L.; Stover, D.R.; Klimkait, T. Effect of polymorphisms on the replicative capacity of protease inhibitor-resistant HIV-1 variants under drug pressure. *Clin. Microbiol. Infect.* **2004**, *10*, 119–126. [CrossRef]
18. Neogi, U.; Sahoo, P.N.; Kumar, R.; De Costa, A.; Shet, A. Characterization of HIV type 1 subtype C protease gene: Selection of L63P mutation in protease inhibitor-naive Indian patients. *AIDS Res. Hum. Retroviruses* **2011**, *27*, 1249–1253. [CrossRef]
19. Svicher, V.; Ceccherini-Silberstein, F.; Erba, F.; Santoro, M.; Gori, C.; Bellocchi, M.C.; Giannella, S.; Trotta, M.P.; d'Arminio Monforte, A.; Antinori, A.; et al. Novel HIV-1 protease mutations potentially involved in resistance to protease inhibitors. *Antimicrob. Agents Chemother.* **2005**, *49*, 2015–2025. [CrossRef]
20. Hornak, V.; Okur, A.; Rizzo, R.C.; Simmerling, C. HIV-1 protease flaps spontaneously open and reclose in molecular dynamics simulations. *Proc. Natl. Acad. Sci. USA* **2006**, *103*, 915–920. [CrossRef]
21. Tóth, G.; Borics, A. Flap opening mechanism of HIV-1 protease. *J. Mol. Graph. Model.* **2006**, *24*, 465–474. [CrossRef]
22. Scott, W.R.P.; Schiffer, C.A. Curling of flap tips in HIV-1 protease as a mechanism for substrate entry and tolerance of drug resistance. *Structure* **2000**, *8*, 1259–1265. [CrossRef] [PubMed]
23. Prinz, J.-H.; Wu, H.; Sarich, M.; Keller, B.; Senne, M.; Held, M.; Chodera, J.D.; Schütte, C.; Noé, F. Markov models of molecular kinetics: Generation and validation. *J. Chem. Phys.* **2011**, *134*, 174105. [CrossRef] [PubMed]
24. Schütte, C.; Noé, F.; Lu, J.; Sarich, M.; Vanden-Eijnden, E. Markov state models based on milestoning. *J. Chem. Phys.* **2011**, *134*, 204105. [CrossRef] [PubMed]
25. Torbeev, V.Y.; Raghuraman, H.; Hamelberg, D.; Tonelli, M.; Westler, W.M.; Perozo, E.; Kent, S.B.H. Protein conformational dynamics in the mechanism of HIV-1 protease catalysis. *Proc. Natl. Acad. Sci. USA* **2011**, *108*, 20982–20987. [CrossRef]
26. Naicker, P.; Achilonu, I.; Fanucchi, S.; Fernandes, M.; Ibrahim, M.A.A.; Dirr, H.W.; Soliman, M.E.S.; Sayed, Y. Structural insights into the South African HIV-1 subtype C protease: Impact of hinge region dynamics and flap flexibility in drug resistance. *J. Biomol. Struct. Dyn.* **2013**, *31*, 1370–1380. [CrossRef]
27. Kervinen, J.; Thanki, N.; Zdanov, A.; Tino, J.; Barrish, J.; Lin, P.F.; Colonno, R.; Riccardi, K.; Samanta, H.; Wlodawer, A. Structural analysis of the native and drug-resistant HIV-1 proteinases complexed with an aminodiol inhibitor. *Protein Pept. Lett.* **1996**, *3*, 399–406.
28. Shapovalov, M.V.; Dunbrack, R.L. A smoothed backbone-dependent rotamer library for proteins derived from adaptive kernel density estimates and regressions. *Structure* **2011**, *19*, 844–858. [CrossRef]
29. Van der Spoel, D.; Lindahl, E.; Hess, B.; Groenhof, G.; Mark, A.E.; Berendsen, H.J.C. GROMACS: Fast, flexible, and free. *J. Comput. Chem.* **2005**, *26*, 1701–1718. [CrossRef]
30. Mark, P.; Nilsson, L. Structure and dynamics of the TIP3P, SPC, and SPC/E water models at 298 K. *J. Phys. Chem. A* **2001**, *105*, 9954–9960. [CrossRef]
31. Huang, J.; MacKerell, A.D. CHARMM36 all-atom additive protein force field: Validation based on comparison to NMR data. *J. Comput. Chem.* **2013**, *34*, 2135–2145. [CrossRef]
32. Hess, B.; Bekker, H.; Berendsen, H.J.C.; Fraaije, J.G.E.M. LINCS: A linear constraint solver for molecular simulations. *J. Comput. Chem.* **1997**, *18*, 1463–1472. [CrossRef]
33. Castrignanò, T.; Gioiosa, S.; Flati, T.; Cestari, M.; Picardi, E.; Chiara, M.; Fratelli, M.; Amente, S.; Cirilli, M.; Tangaro, M.A.; et al. ELIXIR-IT HPC@CINECA: High performance computing resources for the bioinformatics community. *BMC Bioinform.* **2020**, *21*, 352. [CrossRef]
34. Abraham, M.J.; Gready, J.E. Optimization of parameters for molecular dynamics simulation using PME in GROMACS 4.5. *J. Comput. Chem.* **2011**, *32*, 2031–2040. [CrossRef] [PubMed]
35. Bussi, G.; Donadio, D.; Parrinello, M. Canonical sampling through velocity rescaling. *J. Chem. Phys.* **2007**, *126*, 014101. [CrossRef]
36. Parrinello, M.; Rahman, A. Polymorphic transitions in single crystals: A new molecular dynamics method. *J. Appl. Phys.* **1981**, *52*, 7182–7190. [CrossRef]

37. Gowers, R.; Linke, M.; Barnoud, J.; Reddy, T.; Melo, M.; Seyler, S.; Domański, J.; Dotson, D.; Buchoux, S.; Kenney, I.; et al. MDAnalysis: A Python package for the rapid analysis of molecular dynamics simulations. In *Proceedings of the 15th Python in Science Conference, Austin, TX, USA, 11–17 July 2016*; SciPy: Austin, TX, USA, 2016; pp. 98–105.
38. Hekkelman, M.L.; Salmoral, D.Á.; Perrakis, A.; Joosten, R.P. DSSP 4: FAIR annotation of protein secondary structure. *Protein Sci.* **2025**, *34*, e70208. [CrossRef]
39. Grant, B.J.; Rodrigues, A.P.C.; ElSawy, K.M.; McCammon, J.A.; Caves, L.S.D. Bio3D: An R package for the comparative analysis of protein structures. *Bioinformatics* **2006**, *22*, 2695–2696. [CrossRef]